Self-Assembly of a Chiral Cubic Three-Connected Net from the High Symmetry Molecules C_{60} and SnI_4

Daniel B. Straus* and Robert J. Cava*

Department of Chemistry, Princeton University, Princeton, NJ 08544 USA

*Authors to whom correspondence should be addressed. Email: dstraus@princeton.edu, rcava@princeton.edu

Abstract

The design of new chiral materials usually requires stereoselective organic synthesis to create molecules with chiral centers. Less commonly, achiral molecules can self-assemble into chiral materials, despite the absence of intrinsic molecular chirality. Here, we demonstrate the assembly of high-symmetry molecules into a chiral van der Waals structure by synthesizing crystals of $C_{60}(SnI_4)_2$ from icosahedral buckminsterfullerene (C_{60}) and tetrahedral SnI_4 molecules through spontaneous self-assembly. The SnI_4 tetrahedra template the Sn atoms into a chiral cubic three-connected net of the $SrSi_2$ type that is held together by van der Waals forces. Our results represent the remarkable emergence of a self-assembled chiral material from two of the most highly symmetric molecules, demonstrating that almost any molecular, nanocrystalline, or engineered precursor can be considered when designing chiral assemblies.

TOC Graphic

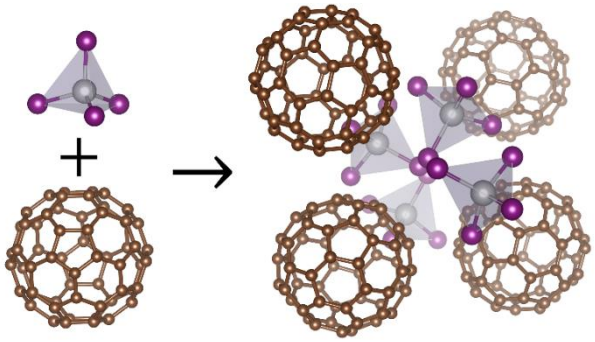

Introduction

Chiral materials are prized for their unique structural, optical, and catalytic properties.[1–6] Most chiral materials are molecules synthesized using stereoselective organic synthesis to imprint chirality through the arrangement of atoms. A molecule is chiral if its mirror image is not superimposable on itself, and enantiomerically pure chiral molecules always form chiral crystals.[7] The chirality of a molecule is maintained even when crystals containing such molecules are dissolved in solution. Another class of chiral materials are three-dimensional covalent or ionic inorganic solids with chiral crystal structures. Examples are the covalent α- and β-quartz, both of which are intrinsically chiral because of the connectivity of their corner-sharing SiO_4 tetrahedra,[8] as well as the ionic $NaClO_3$.[7]

A third class of chiral materials can occur when achiral molecules self-assemble into a chiral material. These molecules are not bonded to one another and are held together by van der Waals forces, and, when dissolved in solution, the achiral building blocks are recovered and the optical activity of the crystal is lost.[7] Chiral molecular materials formed from achiral building blocks greatly expand the phase-space of optically active species because their chirality is not limited by the connectivity of atoms. The achiral molecules making up these chiral crystals usually contain aromatic substituents and are low symmetry and/or planar compounds.[9,10] One-component chiral crystals formed from achiral molecules are relatively common and are reported to make up ~8% of the Cambridge Structural Database,[10] but chiral crystals composed of two or more achiral molecules are scarcely reported.[11–15]

Here we synthesize the chiral van der Waals compound $C_{60}(SnI_4)_2$ from the highly symmetric achiral molecules C_{60} and SnI_4. One of the molecular constituents of our new compound, C_{60}, is in the I_h icosahedral point group (Figure 1a), which is the highest possible

symmetry for a molecule.[16] Further, if a C_{60} molecule freely rotates in a solid like in $C_{60}(SnI_4)_2$, it behaves as if it is spherically symmetric.[17] At room temperature where the C_{60} molecules freely rotate, C_{60} itself crystallizes in an achiral centrosymmetric face-centered cubic (FCC) structure, and below 260 K, where the rotation of C_{60} is frozen, the material undergoes a phase transition to a lower-symmetry but still achiral centrosymmetric simple cubic structure.[18–20] The other molecular constituent of our new compound is SnI_4, which crystallizes as a molecular solid in an achiral centrosymmetric simple cubic structure where each SnI_4 molecule is in the T_d tetrahedral point group (Figure 1b).[21]

Surprisingly, we find that $C_{60}(SnI_4)_2$ self-assembles in the chiral enantiomorphic cubic space group $P4_332$ (#212), which is intrinsically chiral because it has a 4_3-screw axis. The SnI_4 tetrahedra template the Sn atoms to form a chiral three-dimensional three-connected $SrSi_2$-type net, despite the lack of Sn-Sn bonding.[22–24] The formation of a chiral three-connected $SrSi_2$-type net in this type of van der Waals structure is unprecedented because it has previously only been found where the atoms comprising the net are adjacent to one another, such as in extended inorganic solids, metal-organic frameworks, and the hydrogen bonding network of crystalline H_2O_2.[22,25–27] Furthermore, based on our extensive analysis of the Cambridge Structural Database, we believe $C_{60}(SnI_4)_2$ is the first chiral van der Waals crystal assembled from two or more neutral components that each have T_d or greater symmetry. Other chiral C_{60} intercalation compounds have low-symmetry intercalants,[28,29] ambiguous Flack parameters demonstrating the handedness of the structure is not determined,[30] or very high R values indicating further refinement is needed.[31] Existing C_{60} intercalation compounds with tetrahedral intercalants are achiral.[32–34] The emergence of chirality from the combination of these highly symmetric achiral

molecules provides design principles for the three-dimensional chiral self-assembly of molecules, colloidal nanocrystals,[35] and engineered nanostructures.[36]

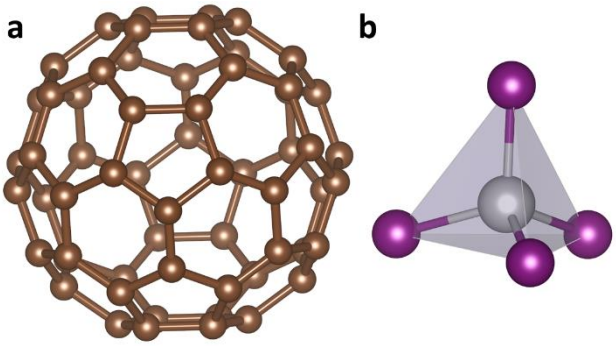

Figure 1: Molecular constituents of $C_{60}(SnI_4)_2$: Individual molecules of (a) C_{60} and (b) SnI_4.[18,21]

Methods

In a typical crystallization, $C_{60}(SnI_4)_2$ is grown in solution by dissolving 20 mg C_{60} (BuckyUSA, >99.5%) and 1000 mg SnI_4 (Alfa-Aesar, >95%) in 40 mL 1,2-dichlorobenzene (Acros Organics, 99%). 200 mL of pentane (Sigma-Aldrich, 98%) is carefully layered on top of the 1,2-dichlorobenzene solution and the jar is sealed and left undisturbed for several weeks while the two layers mix. Two crystal habits form: black hexagonal crystals of $C_{60}(SnI_4)_2$ at the bottom of the jar, and black needle-like crystals on the sides of the jar which have a unit cell corresponding to the C_{60}-pentane intercalation compound $C_{60}(C_5H_{12})$.[37] The amount of $C_{60}(C_5H_{12})$ that crystallizes can be reduced by layering a small amount of benzene on top of 1,2-dichlorobenzene before layering pentane.

Bulk $C_{60}(SnI_4)_2$ is synthesized in the solid-state by sealing C_{60} and SnI_4 in a 1:4 molar ratio in an evacuated quartz tube and heating at 250 °C for 12 hours followed by cooling to room temperature at 3 °C/h. Excess SnI_4 is used to ensure all of the C_{60} reacts. Unreacted SnI_4 is

observed in the X-ray diffraction pattern, so the material is purified two times by sealing in an evacuated quartz tube, heating to 250 °C, and cooling to room temperature at 15 °C/h to sublime off the excess SnI_4.

Crystals are mounted on Kapton MicroLoops (MiTiGen) with Parabar 10312 oil. Single crystal X-ray diffraction data are collected using a Bruker Kappa Apex2 CCD diffractometer using graphite-monochromated Mo Kα radiation with an Oxford Cryostream 700 cryocooler flowing temperature-controlled nitrogen over the crystal. COSMO (Bruker AXS) is used to determine the data collection strategy. Reflections are integrated using SAINT (Bruker AXS), and SADABS (Bruker AXS) scales the data and applies the multi-scan absorption correction. The $P4_332$ space group (#212) is identified through systematic absences using XPREP (Bruker AXS).

The initial solution to the single crystal structure at 295 K is found using the intrinsic phasing method in the SHELXT program,[38] and the structure is refined using the least-squares algorithm in the SHELXL program[39] in the OLEX2 GUI.[40] The absolute configuration of the structure is determined using the anomalous dispersion. The occupancies of the disordered iodine atom I2A and I2B freely refine but are constrained to sum to unity, and their atomic displacement parameters (ADPs) are constrained to be equal using the EADP instruction in SHELXL. The C_{60} molecule is refined by importing the idealized C_{60} molecule from the Molecular Structure Library[41] and removing all C atoms that are not needed for the asymmetric unit. The geometry of the C_{60} asymmetric unit is restrained using the AFIX 9 instruction, and C-C distances in the six-membered rings adjacent to the asymmetric unit in the grown structure are restrained using the SADI instruction to regularize the C_{60} molecule. The ADPs of the C atoms

are restrained with the DELU instruction. Visualizations of all structures are created using VESTA.[42]

Powder X-ray diffraction data are collected on a Bruker D8 Advance Eco diffractometer in Bragg-Brentano geometry using Cu Kα radiation with a LYNXEYE 1D strip detector. Thermogravimetric analysis (TGA) is conducted using a TA Instruments SDT Q600 under flowing argon. Diffuse reflectance spectra are collected using an Agilent Cary 5000 UV-Vis-NIR absorption spectrometer with an Agilent Internal DRA-2500 diffuse reflectance accessory. Materials are diluted to 2-5% w/w with dry MgO, and dry MgO is used as the reflectance standard. Pseudoabsorbance spectra are generated from diffuse reflectance spectra using the Kubelka-Munk function.[43] Raman scattering spectra are collected using a Thermo-Fisher DXR Smart Raman spectrometer equipped with a 780 nm HP laser.

Results and Discussion

C_{60} and SnI_4 are both molecular solids, where van der Waals forces hold the molecules together in their crystal structures. C_{60} and SnI_4 co-crystallize to yield the buckminsterfullerene intercalation compound $C_{60}(SnI_4)_2$, which is a van der Waals compound like its crystalline parent materials. $C_{60}(SnI_4)_2$ crystallizes in the chiral enantiomorphic cubic space group $P4_332$ (#212) (Figure 2a and Table 1). The chiral 4_3 screw axis is highlighted in Figure 2b. The absolute configuration of the measured $C_{60}(SnI_4)_2$ crystal is determined using the anomalous dispersion, evidenced by the Flack parameter of -0.08(3).[7] One of the two independent iodine atoms resolves with disorder and has refined occupancies of 0.752(9) and 0.248(9). This disorder is omitted for clarity in Figure 2a-b; the structure with disorder and the asymmetric unit are shown in Figure S1. TGA of a single crystal (Figure S2) indicates 63% of the mass is lost when heated above 225

°C, consistent with a loss of two SnI_4 molecules which comprise 63.5% of the mass of $C_{60}(SnI_4)_2$. While the Sn and I atoms have well-behaved ADPs, the C atoms have nearly two-dimensional oblate and prolate ADPs. Abnormal ADPs usually indicate a problem with the structural model, but here they are expected because the C atoms are constrained to the surface of the C_{60} ball which we hypothesize is rotating within the crystal like in pure C_{60} at room temperature.[17] The shortest C_{60} center-to-center distance in $C_{60}(SnI_4)_2$ is 10.14 Å, which is only slightly larger than the 10.02 Å distance in room temperature FCC C_{60}.[44] However, in $C_{60}(SnI_4)_2$ each C_{60} only has six nearest neighbors compared to twelve in FCC C_{60}; the C_{60} frameworks in $C_{60}(SnI_4)_2$ and FCC C_{60} are shown in Figure S3. It is possible that in some preparations single crystals of $C_{60}(SnI_4)_2$ may crystallize in the space group $P4_132$ (#213), which is the enantiomer of $P4_332$ (#212).

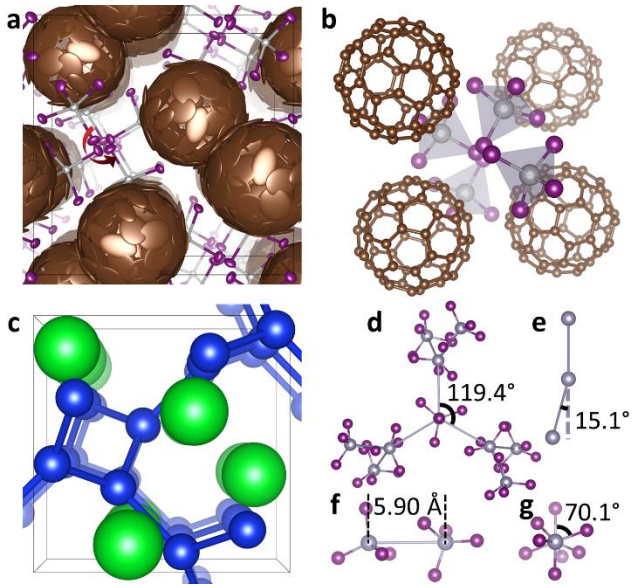

Figure 2: Structural characterization. (a) Structure of $C_{60}(SnI_4)_2$ with C (brown), Sn (grey), and I (purple) and atoms represented as 50% probability thermal ellipsoids. The chiral 4_3 screw axis is indicated by the red arrow. (b) Detail of chiral 4_3 screw axis. (c) Structure of $SrSi_2$ with Sr (green) and Si (blue).[45] (d) Top and (e) side view of Sn net, with depictions of adjacent SnI_4 tetrahedra (f) along and (g) down the Sn-Sn axis. Nearest-neighbor Sn-Sn distances are shown as bonds in (d-g).

Table 1: Crystallographic Collection and Structural Parameters

Empirical formula	$C_{60}Sn_2I_8$
Formula weight	1973.18
Temperature (K)	295
Crystal system	cubic
Space group	$P4_332$ (#212)
a (Å)	16.5593(6)
Volume (Å^3)	4540.7(5)
Z	4
ρcalc (g/cm^3)	2.886
μ (mm^{-1})	6.585
F(000)	3536
Crystal size (mm^3)	0.31 × 0.301 × 0.164
Radiation	Mo Kα (λ = 0.71073 Å)
2Θ range for data collection (°)	3.478 to 59.152
Index ranges	-19 ≤ h ≤ 12, -8 ≤ k ≤ 22, -21 ≤ l ≤ 12
Reflections collected	8784
Independent reflections	2132 [R_{int} = 0.0228, R_{sigma} = 0.0246]
Data/restraints/parameters	2132/80/88
Goodness-of-fit on F^2	1.067
Final R indexes [I>=2σ(I)]	R_1 = 0.0405, wR_2 = 0.0957
Final R indexes [all data]	R_1 = 0.0518, wR_2 = 0.1012
Largest diff. peak/hole (e Å^{-3})	0.85/-0.70
Flack parameter	-0.08(3)

$C_{60}(SnI_4)_2$ adopts the $SrSi_2$ structure type (Figure 2c), where the center of each C_{60} molecule is at the Sr position (green, Figure 2c) and an Sn atom occupies the Si position (blue, Figure 2c). In $SrSi_2$, the Si atoms (blue, Figure 2c) form a chiral three-dimensional three-connected net with a Wells classification of (10,3)-a, signifying each Si atom is bonded to 3 other Si atoms, and the smallest cycle in the net is a 10-membered ring.[22–24] This net is also known as the **srs** net after $SrSi_2$.[24,27] In addition to being found in $SrSi_2$ and similar inorganic structures, the chiral three-connected **srs** net is also found in metal-organic frameworks as well as in the hydrogen bonding network of H_2O_2.[22,25–27] Remarkably, the Sn atoms in $C_{60}(SnI_4)_2$ form a chiral three-connected **srs** net despite not being adjacent to one another because the net is

templated by the orientation of the SnI_4 tetrahedra. Each Sn atom sits on a site with threefold rotational symmetry (Figure 2d). The four Sn atoms in each repeating unit are nearly planar, deviating by 15.08(2)° (Figure 2e), and have an internal angle of 119.42(1)° compared to the ideal 120° for the undistorted **srs** net.[22,45] The net in $C_{60}(SnI_4)_2$ is less distorted than in $SrSi_2$, where the internal angle is 117.8° with a 29.4° deviation from planar.[45] Each Sn atom is separated from its three nearest-neighbors by 5.9065(7) Å (Figure 2f), and the I atoms are partially staggered when looking down the Sn-Sn axis (Figure 2g).

The packing of SnI_4 tetrahedra in $C_{60}(SnI_4)_2$ is markedly different than in pure SnI_4. In crystalline SnI_4,[46] each SnI_4 tetrahedron has a single nearest-neighbor that has staggered I atoms, a Sn-Sn distance of 5.465(3) Å, and a dihedral angle of 60° (Figure S4a). They each also have 6 next nearest-neighbors with a Sn-Sn distance of 6.819(1) Å and dihedral angles of 30.62(9)° (Figure S4b), and there also 6 next-next nearest neighbors that are equivalent under translation, are separated by 7.514(2) Å, and have eclipsed I atoms (Figure S4c).

The ratio γ between the size of small and large atoms in binary structures has been used to rationalize and predict superlattice structures formed from binary mixtures of monodisperse quasi-spherical nanocrystals,[35] and the self-assembly of C_{60} and SnI_4 into the $SrSi_2$ structure type is consistent with this principle. In $SrSi_2$, γ is 0.55. A phase of $BaSi_2$ adopts the $SrSi_2$ structure[47] and γ is 0.53. Here, we approximate the radius of C_{60} to be 5.01 Å, which is half of the center-to-center distance in FCC C_{60}.[44] Computing the size of SnI_4 is difficult because tetrahedra are not spheres, and the three Sn-Sn distances in pure SnI_4 demonstrate that the effective size of a SnI_4 tetrahedron depends on the packing. In $C_{60}(SnI_4)_2$, there is only one geometry between adjacent SnI_4 tetrahedra, so we approximate the radius of SnI_4 by taking half of the Sn-Sn distance (2.95 Å). Using these approximations, we find γ to be 0.59, only 7% larger than γ in $SrSi_2$.

γ is not the only predictor of a structure type because a ratio of 0.59 is also within the range of stability for the AlB_2 structure type,[35] where the B atoms form another type of three-connected net. In AlB_2, however, the net is a planar honeycomb (graphene) net rather than a chiral three-dimensional **srs** net. In $C_{60}(SnI_4)_2$, forming a planar net would require rotations about Sn-Sn axes that would cause eclipsed I atoms on some adjacent SnI_4 tetrahedra. An eclipsed geometry would require longer Sn-Sn distances and would likely break the 3-fold rotational symmetry, and longer Sn-Sn distances would not minimize the free volume in the structure. We therefore hypothesize that the chiral three-connected **srs** net is templated by the tetrahedral shape of the SnI_4 molecules, suggesting that appropriately sized and shaped[48] colloidal nanocrystals and/or engineered nanostructures[36] may also be able to self-assemble into chiral assemblies with the $SrSi_2$ structure.

$C_{60}(SnI_4)_2$ can also be synthesized directly by heating C_{60} with an excess of SnI_4 (to ensure that all C_{60} reacts) in an evacuated quartz tube and subsequently subliming away the excess SnI_4. Direct synthesis in the solid-state results in the formation of a powder rather than single crystals, and the X-ray diffraction pattern of the powder is shown in dark red in Figure S5 with a simulated pattern from the single crystal structure in black. The chiral three-connected **srs** net still forms under solid-state synthesis. No excess SnI_4 is observed in the pattern. TGA on the powder reveals the presence of an additional 10% of SnI_4 compared to the crystals, resulting in an empirical formula of $C_{60}(SnI_4)_{2.2}$ (Figure S6), which could be the result of excess SnI_4 not incorporated into the crystal structure even though it is not observed in the diffraction pattern.

Upon cooling below 260 K, a reversible phase transition occurs that may disrupt the chiral three-connected **srs** net. We follow this transition crystallographically by observing the appearance of reflections that are systematically absent in $P4_332$ (Figure 3). Pure C_{60} also

undergoes a phase transition upon cooling below 255-260 K where the C_{60} molecules rotationally order, resulting in a change from a FCC to a primitive cubic structure.[19,20] Given the nearly identical temperatures of the phase transitions in C_{60} and $C_{60}(SnI_4)_2$, we hypothesize that a similar rotational ordering of C_{60} occurs in $C_{60}(SnI_4)_2$, which breaks the 4_3 screw axis because the C_{60} molecules no longer behave as spherical shells and become inequivalent by symmetry. However, we are unable to solve the structure of $C_{60}(SnI_4)_2$ below 260 K because of twinning, which is indicated at 100 K by the $|E^2 - 1|$ statistic of 0.555 (compared to 0.541 for a perfectly twinned acentric crystal) as well as the cumulative intensity distribution (Figure S7).[49,50] Determination of the low temperature crystal structure is beyond the scope of the current study.

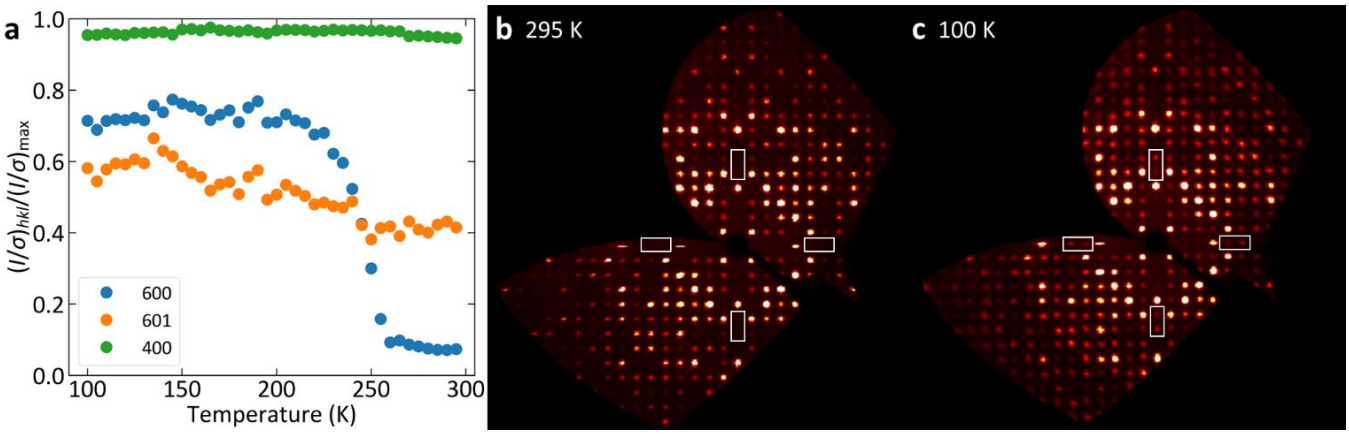

Figure 3: Phase transition. (a) Temperature-dependent intensity of selected allowed ((601) and (400)) and systematically absent (600) reflections. Synthesized precession images of h0l plane at (b) 295 K and (c) 100 K. White boxes highlight systematically absent reflections (h00 = 0k0 = 00l ≠ 4n) at 295 K that appear prominently at temperatures below 260 K.

Optically, $C_{60}(SnI_4)_2$ behaves similarly to a combination of pure C_{60} and SnI_4, which is expected because $C_{60}(SnI_4)_2$ is a van der Waals compound composed of discrete C_{60} and SnI_4 molecules. Raman scattering spectra (Figure 4a) demonstrate that the C_{60} and SnI_4 molecules only weakly interact in $C_{60}(SnI_4)_2$ because its Raman spectrum is almost identical to the combination of the spectra of pure C_{60} and SnI_4. One notable difference is the region between

475 and 575 cm^{-1} (Figure 4a, inset). In C_{60}, the 493 cm^{-1} a_g vibrational mode[51] is known to shift to higher frequency upon reduction to C_{60}^- and to lower frequency upon oxidation to C_{60}^+,[52] and the shift of this mode to lower frequency in $C_{60}(SnI_4)_2$ suggests that that C_{60} may be oxidized. Another difference is that a weak peak[53] observed at 564 cm^{-1} in C_{60} shifts to 529 cm^{-1} in $C_{60}(SnI_4)_2$. The absorption onset of $C_{60}(SnI_4)_2$ matches pure C_{60} near the band edge, further indicating that C_{60} and SnI_4 only weakly interact. Pseudoabsorbance spectra are shown in Figure 4b. Whether synthesized in solution or in the solid-state, $C_{60}(SnI_4)_2$ has a direct band gap of 1.76(1) eV, almost identical to the 1.74(1) eV band gap we find for pure C_{60} (Figure S8). Interestingly, $C_{60}(SnI_4)_2$ has a weak transition around 1.5 eV shown in the inset of Figure 3A that is absent in pure C_{60} and SnI_4. It is possible that this is another indication of oxidation of C_{60} and corresponds to the transition from the $g_g + h_g$ to h_u molecular orbitals of C_{60},[54] though the energy of the observed transition is larger than the 1.26 eV one electron oxidation potential of C_{60} measured in solution by cyclic voltammetry.[55] Above the band edge, $C_{60}(SnI_4)_2$ has increased absorption in the range where pure SnI_4 absorbs, and the solid-state synthesized sample with an empirical formula $C_{60}(SnI_4)_{2.2}$ absorbs more strongly than the solution-synthesized sample, consistent with the presence of additional SnI_4. Detailed electronic structure calculations are needed to understand the interaction between C_{60} and SnI_4 molecules in $C_{60}(SnI_4)_2$.

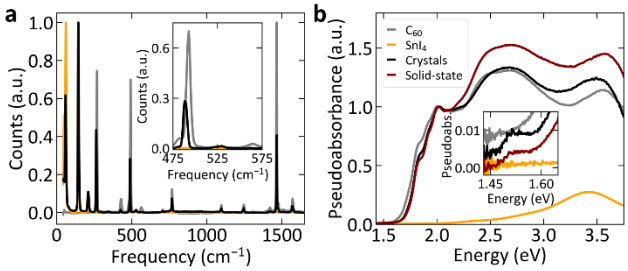

Figure 4: Optical characterization. (a) Raman scattering spectra of C_{60} (grey), SnI_4 (orange), and $C_{60}(SnI_4)_2$ crystallized from solution (black). (b) Pseudoabsorbance spectra of C_{60} (grey), SnI_4 (orange), and $C_{60}(SnI_4)_2$ crystallized from solution (black) and synthesized in the solid-state (dark red).

Conclusion

The synthesis of $C_{60}(SnI_4)_2$ indicates that highly symmetric achiral molecules can crystallize into a multi-component chiral van der Waals structure by self-assembly that includes a chiral three-connected **srs** net. While the C_{60} and SnI_4 components maintain their discrete molecular character, shifts in the energy of vibrational modes and the appearance of a sub-band gap optical transition in $C_{60}(SnI_4)_2$ suggest that C_{60} may be slightly oxidized, indicating a small degree of charge transfer from C_{60} to SnI_4. This discovery expands the library of molecules that can be used to form multi-component chiral assemblies as well as demonstrating that tetrahedra can template the chiral self-assembly of a binary material. Topologically, we demonstrate that a chiral three-connected **srs** net can form, even though the members of the net do not directly contact each other. Our results lay the framework for the design and creation of novel optical and catalytic materials formed by the self-assembly of highly symmetric precursors. In addition to molecules, the principles developed herein can guide the design of mixtures of tetrahedral[48] and spherical nanoparticles and/or engineered nanostructures[36] that will self-assemble into chiral $SrSi_2$-type structures.

Supporting Information

The Supporting Information is available free of charge at [PLACEHOLDER]

Single crystal X-ray crystallographic data have been deposited at the Cambridge Crystallographic Data Centre under deposition number CCDC 1997295 and can be accessed at https://www.ccdc.cam.ac.uk/structures/ as well as in the Supporting Information (CIF)

Figures S1-S8: Additional structural depictions, TGA, cumulative intensity distributions of single crystal X-ray diffraction data, band gap determination (PDF)

Acknowledgments

We thank Dr. Robert A. Pascal for discussion on chiral crystal structures and Dr. Weiwei Xie for conversations on polar intermetallics. This work is supported by the Gordon and Betty Moore Foundation under grant GBMF-4412.

References

(1) Kitaev, V. Chiral Nanoscale Building Blocks—from Understanding to Applications. *J. Mater. Chem.* **2008**, *18*, 4745.

(2) Song, C. E.; Lee, S. G. Supported Chiral Catalysts on Inorganic Materials. *Chem. Rev.* **2002**, *102*, 3495–3524.

(3) Adams, J. B.; Filice, A. L. Spectral Reflectance 0.4 to 2.0 Microns of Silicate Rock Powders. *J. Geophys. Res.* **1967**, *72*, 5705–5715.

(4) Soai, K.; Osanai, S.; Kadowaki, K.; Yonekubo, S.; Shibata, T.; Sato, I. D - and l -Quartz-Promoted Highly Enantioselective Synthesis of a Chiral Organic Compound. *J. Am. Chem. Soc.* **1999**, *121*, 11235–11236.

(5) Smerdon, J. A.; Rankin, R. B.; Greeley, J. P.; Guisinger, N. P.; Guest, J. R. Chiral "Pinwheel" Heterojunctions Self-Assembled from C 60 and Pentacene. *ACS Nano* **2013**, *7*, 3086–3094.

(6) Xu, B.; Tao, C.; Cullen, W. G.; Reutt-Robey, J. E.; Williams, E. D. Chiral Symmetry Breaking in Two-Dimensional C 60 - ACA Intermixed Systems. *Nano Lett.* **2005**, *5*, 2207–2211.

(7) Flack, H. D. Chiral and Achiral Crystal Structures. *Helv. Chim. Acta* **2003**, *86*, 905–921.

(8) Tucker, M. G.; Keen, D. A.; Dove, M. T. A Detailed Structural Characterization of Quartz on Heating through the α–β Phase Transition. *Mineral. Mag.* **2001**, *65*, 489–507.

(9) Liu, M.; Zhang, L.; Wang, T. Supramolecular Chirality in Self-Assembled Systems. *Chem. Rev.* **2015**, *115*, 7304–7397.

(10) Matsuura, T.; Koshima, H. Introduction to Chiral Crystallization of Achiral Organic Compounds: Spontaneous Generation of Chirality. *J. Photochem. Photobiol. C*

Photochem. Rev. **2005**, *6*, 7–24.

(11) Tan, T. F.; Han, J.; Pang, M. L.; Song, H. Bin; Ma, Y. X.; Meng, J. Ben. Achiral Benzoic Acid Derivatives as Chiral Cocrystal Building Blocks in Supramolecular Chemistry: Adducts with Organic Amines. *Cryst. Growth Des.* **2006**, *6*, 1186–1193.

(12) Koshima, H.; Miyauchi, M. Polymorphs of a Cocrystal with Achiral and Chiral Structures Prepared by Pseudoseeding: Tryptamine/Hydrocinnamic Acid. *Cryst. Growth Des.* **2001**, *1*, 355–357.

(13) Koshima, H.; Nakagawa, T.; Matsuura, T.; Miyamoto, H.; Toda, F. Synthesis, Structure, and Discrimination of Chiral Bimolecular Crystals by Using Diphenylacetic Acid and Aza Aromatic Compounds. *J. Org. Chem.* **1997**, *62*, 6322–6325.

(14) Koshima, H.; Matsuura, T. Chiral Bimolecular Crystallization of Achiral Molecules. *Mol. Cryst. Liq. Cryst. Sci. Technol. Sect. A Mol. Cryst. Liq. Cryst.* **1998**, *313*, 65–74.

(15) Koshima, H.; Matsuura, T. Chiral Crystallization of Achiral Organic Compounds. Generation of Chirality without Chiral Environment. (Part 2). *J. Synth. Org. Chem. Japan* **1998**, *56*, 466–477.

(16) Rassat, A. Chirality and Symmetry Aspects of Spheroarenes, Including Fullerenes. *Chirality* **2001**, *13*, 395–402.

(17) Fischer, J. E.; Heiney, P. A.; McGhie, A. R.; Romanow, W. J.; Denenstein, A. M.; McCauley, J. P.; Smith III, A. B. Compressibility of Solid C60. *Science* **1991**, *252*, 1288–1290.

(18) David, W. I. F.; Ibberson, R. M.; Matthewman, J. C.; Prassides, K.; Dennis, T. J. S.; Hare, J. P.; Kroto, H. W.; Taylor, R.; Walton, D. R. M. Crystal Structure and Bonding of Ordered C60. *Nature* **1991**, *353*, 147–149.

(19) David, W. I. F.; Ibberson, R. M.; Dennis, T. J. S.; Hare, J. P.; Prassides, K. Structural Phase Transitions in the Fullerene C 60. *Europhys. Lett.* **1992**, *18*, 735–736.

(20) Heiney, P. A. Structure, Dynamics and Ordering Transition of Solid C60. *J. Phys. Chem. Solids* **1992**, *53*, 1333–1352.

(21) Dickinson, R. G. The Crystal Structure of Tin Tetra-Iodide. *J. Am. Chem. Soc.* **1923**, *45*, 958–962.

(22) Wells, A. F. *Three-Dimensional Nets and Polyhedra*; Wiley: New York, 1977.

(23) Ienco, A.; Proserpio, D. M.; Hoffmann, R. Main Group Element Nets to a T. *Inorg. Chem.* **2004**, *43*, 2526–2540.

(24) Zheng, C.; Hoffmann, R. Conjugation in the Three-Connected Net: The AIB2and ThSi2 Structures and Their Transition-Metal Derivatives. *Inorg. Chem.* **1989**, *28*, 1074–1080.

(25) Carlucci, L.; Ciani, G.; Proserpio, D. M.; Sironi, A. A Three-Dimensional, Three-Connected Cubic Network of the SrSi2 Topological Type in Coordination Polymer Chemistry: [Ag(Hmt)](PF6)·H2O (Hmt = Hexamethylenetetraamine). *J. Am. Chem. Soc.* **1995**, *117*, 12861–12862.

(26) Yaghi, O. M.; Davis, C. E.; Li, G.; Li, H. Selective Guest Binding by Tailored Channels in a 3-D Porous Zinc(II)−Benzenetricarboxylate Network. *J. Am. Chem. Soc.* **1997**, *119*, 2861–2868.

(27) Hyde, S. T.; O'Keeffe, M.; Proserpio, D. M. A Short History of an Elusive yet Ubiquitous Structure in Chemistry, Materials, and Mathematics. *Angew. Chemie - Int. Ed.* **2008**, *47*, 7996–8000.

(28) Penicaud, A.; Boubekeur, K.; Kotov, A. I.; Yagubskii, E. B. Novel Infinite Three-Dimensional Network of Neutral Fullerene Molecules in (C 60) 8 (Twin-TDAS) 6. *Acta Crystallogr. Sect. B Struct. Sci.* **2000**, *56*, 497–500.

(29) Szymański, M. P.; Jędrzejewska, H.; Wierzbicki, M.; Szumna, A. On the Mechanism of Mechanochemical Molecular Encapsulation in Peptidic Capsules. *Phys. Chem. Chem. Phys.* **2017**, *19*, 15676–15680.

(30) Konarev, D. V.; Kovalevsky, A. Y.; Khasanov, S. S.; Saito, G.; Lopatin, D. V.; Umrikhin, A. V.; Otsuka, A.; Lyubovskaya, R. N. Synthesis, Crystal Structures, Magnetic Properties and Photoconductivity of C60 and C70 Complexes with Metal Dialkyldithiocarbamates M(R2dtc)x, Where M = CuII, CuI, AgI, ZnII, CdII, HgII, Mn II, NiII, and PtII; R = Me, Et, and NPr. *Eur. J. Inorg. Chem.* **2006**, No. 9, 1881–1895.

(31) Boeyens, J. C. A.; Ramm, M.; Zobel, D.; Luger, P. Static Disorder and Packing in Two Orthorhombic Crystal Structures of Fullerene Inclusion Compounds. *South African J. Chem.* **1997**, *50*, 28–33.

(32) Locke, I. W.; Darwish, A. D.; Kroto, H. W.; Prassides, K.; Taylor, R.; Walton, D. R. M. Phosphorus/Buckminsterfullerene Intercalation Compounds, C60(P4)2. *Chem. Phys. Lett.* **1994**, *225*, 186–190.

(33) Troyanov, S. I.; Kemnitz, E. Structure of Fullerene C60 in the Crystalline Adduct C60 · 3TiCl4. *Russ. J. Inorg. Chem.* **2001**, *46*, 1547–1552.

(34) Céolin, R.; Agafonov, V.; André, D.; Dworkin, A.; Szwarc, H.; Dugué, J.; Keita, B.; Nadjo, L.; Fabre, C.; Rassat, A. Fullerene C60, 2CCl4 Solvate. A Solid-State Study. *Chem. Phys. Lett.* **1993**, *208*, 259–262.

(35) Shevchenko, E. V; Talapin, D. V; Murray, C. B.; O'Brien, S. Structural Characterization of Self-Assembled Multifunctional Binary Nanoparticle Superlattices. *J. Am. Chem. Soc.* **2006**, *128*, 3620–3637.

(36) Zhang, M.; Guo, J.; Yu, Y.; Wu, Y.; Yun, H.; Jishkariani, D.; Chen, W.; Greybush, N. J.; Kübel, C.; Stein, A.; et al. 3D Nanofabrication via Chemo-Mechanical Transformation of

Nanocrystal/Bulk Heterostructures. *Adv. Mater.* **2018**, *30*, 1800233.

(37) Chancellor, C. J.; Bowles, F. L.; Franco, J. U.; Pham, D. M.; Rivera, M.; Sarina, E. A.; Ghiassi, K. B.; Balch, A. L.; Olmstead, M. M. Single-Crystal X-Ray Diffraction Studies of Solvated Crystals of C 60 Reveal the Intermolecular Interactions between the Component Molecules. *J. Phys. Chem. A* **2018**, *122*, 9626–9636.

(38) Sheldrick, G. M. SHELXT – Integrated Space-Group and Crystal-Structure Determination. *Acta Crystallogr. Sect. A Found. Adv.* **2015**, *71*, 3–8.

(39) Sheldrick, G. M. Crystal Structure Refinement with SHELXL . *Acta Crystallogr. Sect. C Struct. Chem.* **2015**, *71*, 3–8.

(40) Dolomanov, O. V.; Bourhis, L. J.; Gildea, R. J.; Howard, J. A. K.; Puschmann, H. OLEX2 : A Complete Structure Solution, Refinement and Analysis Program. *J. Appl. Crystallogr.* **2009**, *42*, 339–341.

(41) Guzei, I. A. An Idealized Molecular Geometry Library for Refinement of Poorly Behaved Molecular Fragments with Constraints. *J. Appl. Crystallogr.* **2014**, *47*, 806–809.

(42) Momma, K.; Izumi, F. VESTA 3 for Three-Dimensional Visualization of Crystal, Volumetric and Morphology Data. *J. Appl. Crystallogr.* **2011**, *44*, 1272–1276.

(43) Hecht, H. G. The Interpretation of Diffuse Reflectance Spectra. *J. Res. Natl. Bur. Stand. Sect. A Phys. Chem.* **1976**, *80A*, 567.

(44) Fischer, J. E. Structure and Dynamics of Solid C60 and Its Intercalation Compounds. *Mater. Sci. Eng. B* **1993**, *19*, 90–99.

(45) Evers, J. Transformation of Three-Dimensional Three-Connected Silicon Nets in SrSi2. *J. Solid State Chem.* **1978**, *24*, 199–207.

(46) Reuter, H.; Pawlak, R. Zinnhalogenverbindungen. II. Die Molekül- Und Kristallstrukturen von Zinn(IV)-Bromid Und -Iodid. *Zeitschrift für Krist. - Cryst. Mater.* **2001**, *216*, 34–38.

(47) Evers, J.; Oehlinger, G.; Weiss, A. Solid Solutions M1−xSrxSi2 (M = Ca, Eu, Ba) and BaSi2−yGey with SrSi2-Type Structure. *J. Less Common Met.* **1980**, *69*, 399–402.

(48) Narayanan, R.; El-Sayed, M. A. Effect of Nanocatalysis in Colloidal Solution on the Tetrahedral and Cubic Nanoparticle SHAPE: Electron-Transfer Reaction Catalyzed by Platinum Nanoparticles. *J. Phys. Chem. B* **2004**, *108*, 5726–5733.

(49) Yeates, T. O.; Tsai, Y. Detecting Twinning by Merohedry. In *International Tables for Crystallography Vol. F*; Arnold, E., Himmel, D. M., Rossmann, M. G., Eds.; International Union of Crystallography: Chester, England, 2012; pp 311–316.

(50) Dauter, Z. Twinned Crystals and Anomalous Phasing. *Acta Crystallogr. - Sect. D Biol. Crystallogr.* **2003**, *59*, 2004–2016.

(51) Eklund, P. C.; Ping, Z.; Kai-An, W.; Dresselhaus, G.; Dresselhaus, M. S. Optical Phonon Modes in Solid and Doped C60. *J. Phys. Chem. Solids* **1992**, *53*, 1391–1413.

(52) Fulara, J.; Jakobi, M.; Maier, J. P. Electronic and Infrared Spectra of C+60 and C-60 in Neon and Argon Matrices. *Chem. Phys. Lett.* **1993**, *211*, 227–234.

(53) Dennis, T. J.; Hare, J. P.; Kroto, H. W.; Taylor, R.; Walton, D. R. M.; Hendra, P. J. The Vibrational Raman Spectra of C60 and C70. *Spectrochim. Acta Part A Mol. Spectrosc.* **1991**, *47*, 1289–1292.

(54) Haddon, R. C. Electronic Structure, Conductivity and Superconductivity of Alkali Metal Doped C60. *Acc. Chem. Res.* **1992**, *25*, 127–133.

(55) Xie, Q.; Arias, F.; Echegoyen, L. Electrochemically-Reversible, Single-Electron Oxidation of C60 and C70. *J. Am. Chem. Soc.* **1993**, *115*, 9818–9819.

Supporting Information: Self-Assembly of a Chiral Cubic Three-Connected Net from the High Symmetry Molecules C_{60} and SnI_4

Daniel B. Straus* and Robert J. Cava*

Department of Chemistry, Princeton University, Princeton, NJ 08544 USA

*Authors to whom correspondence should be addressed. Email: dstraus@princeton.edu, rcava@princeton.edu

Additional Figures

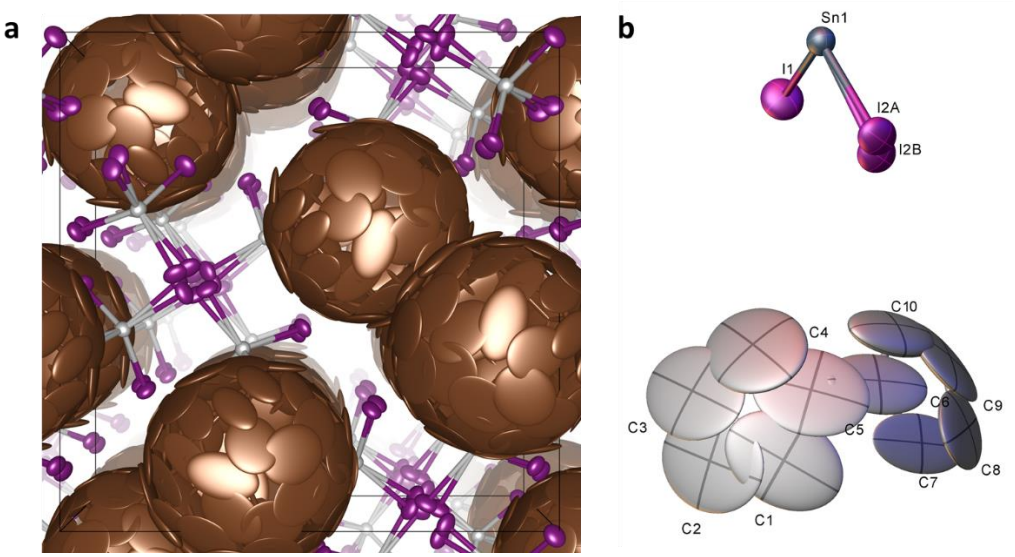

Figure S1: (a) $C_{60}(SnI_4)_2$ with both disordered I atoms, and (b) asymmetric unit. Atoms are represented as 50% probability thermal ellipsoids. (B) created using OLEX2.

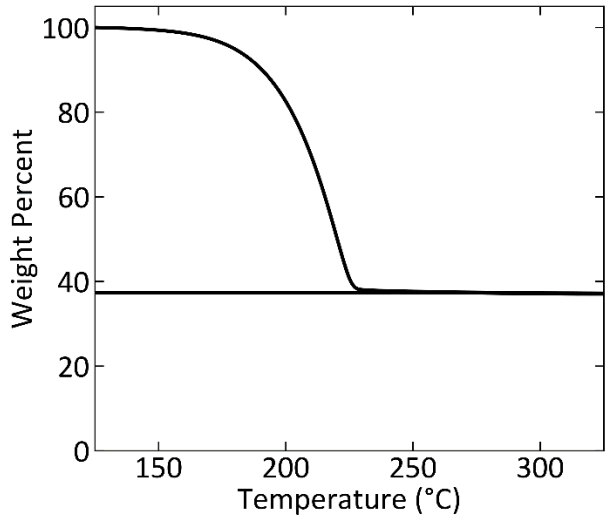

Figure S2: TGA of $C_{60}(SnI_4)_2$ single crystal heated at 0.5 °C/min.

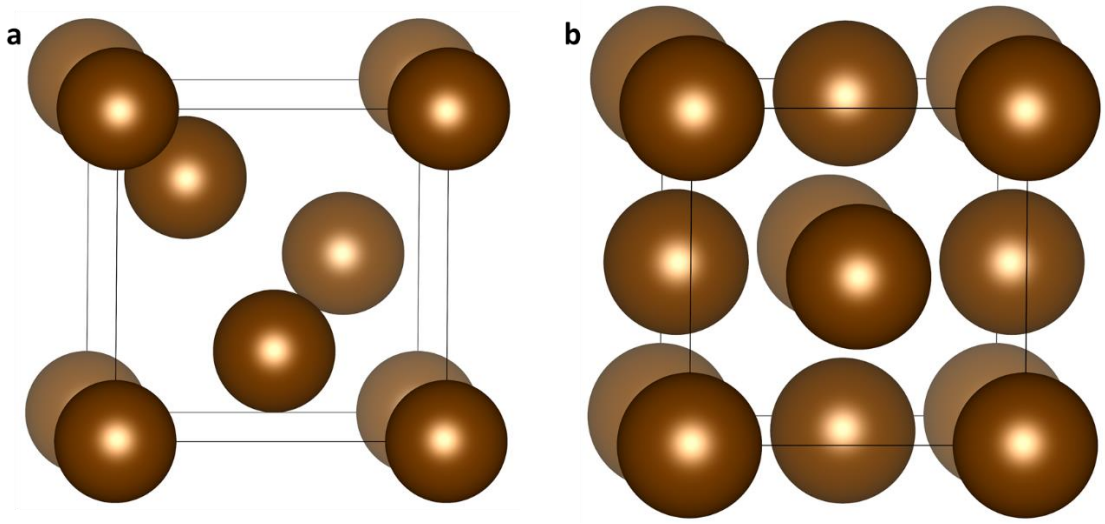

Figure S3: (a) The C_{60} atoms in $C_{60}(SnI_4)_2$ represented as spheres. The origin of the unit cell is shifted by (1/8, 1/8, 1/8) to locate a C_{60} at each corner. (b) The C_{60} atoms in FCC C_{60} represented as spheres.

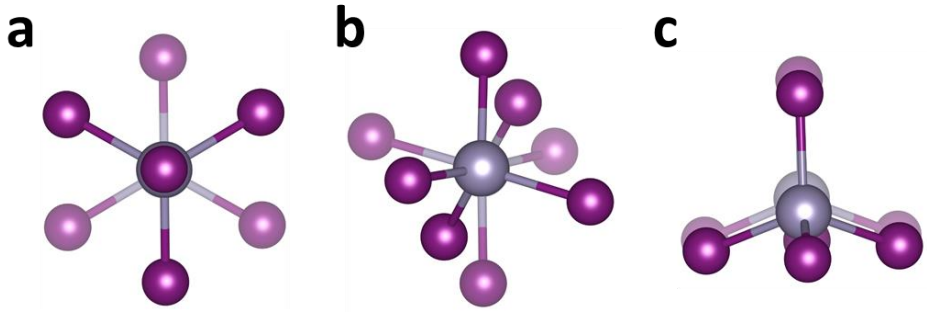

Figure S4: Views of (a) nearest, (b) next-nearest, and (c) next-next-nearest neighbor SnI_4 tetrahedra down Sn-Sn axis in crystalline SnI_4.

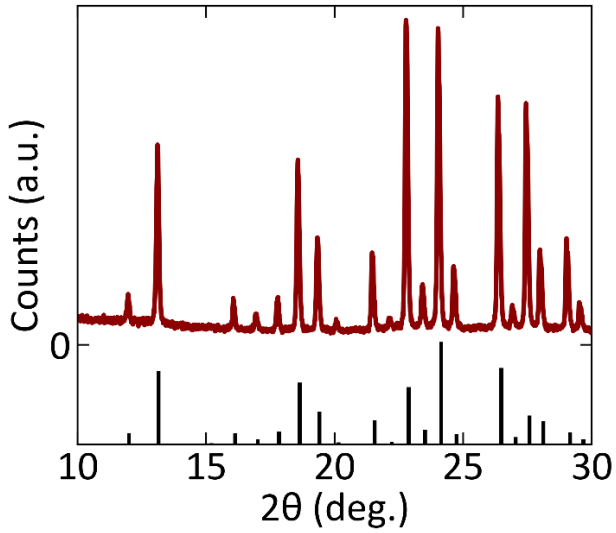

Figure S5: X-ray diffraction pattern of $C_{60}(SnI_4)_2$ synthesized by a solid-state method (dark red) with simulated powder diffraction pattern from single crystal structure (black).

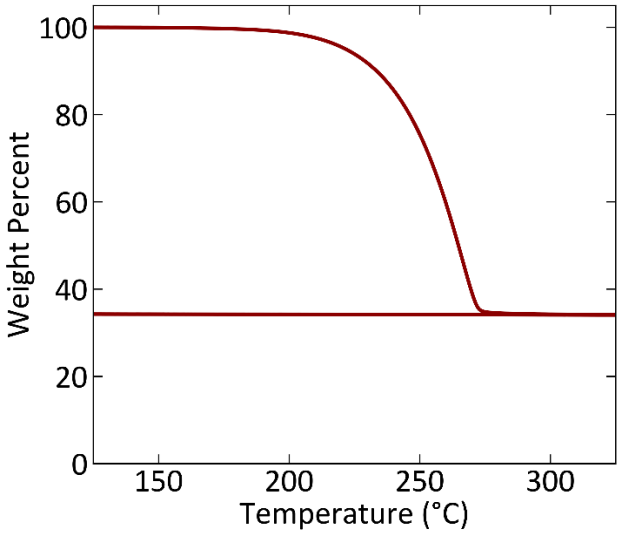

Figure S6: TGA of $C_{60}(SnI_4)_2$ powder from solid-state synthesis heated at 10 °C/min.

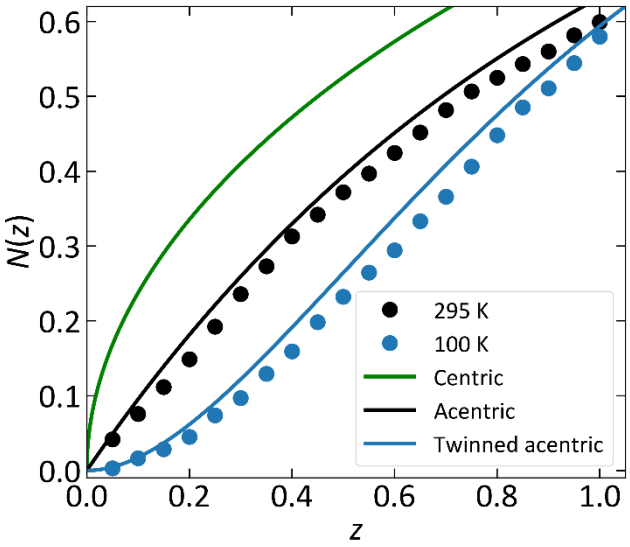

Figure S7: Cumulative intensity distribution for single crystal X-ray diffraction data at 295 K (black circles) and 100 K (blue circles) with ideal distributions for centric (green line), acentric (black line), and twinned acentric (blue line) crystals.

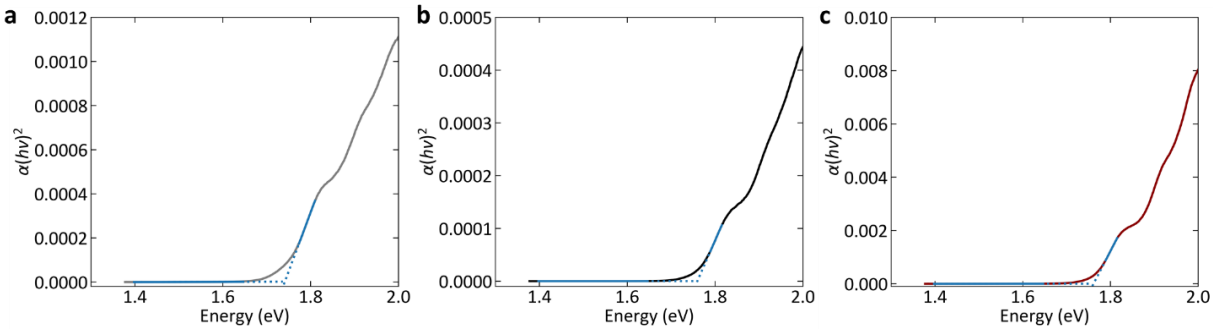

Figure S8: Tauc plots of (a) C_{60} and $C_{60}(SnI_4)_2$ synthesized (b) in solution and (c) in the solid-state.